Spray and Thermal Analysis of Pressure and Air Atomized Nozzles for Electronic Cooling

Monu Kumar [1], Viraj Dusane[1], Arvind Pattamatta[1*], Marco Marengo[2]
[1]Department of Mechanical Engineering, IIT Madras, Chennai-600036, India
[2]Department of Thermal Physics, University of Pavia, Italy.
*Corresponding Author: arvindp@iitm.ac.in

Abstract - This study investigates the effectiveness of spray cooling for managing high heat generation in modern electronics, comparing the performance of two different nozzle types pressure atomized nozzles (PAN) and air atomized nozzles (AAN) . Our experimental setup consists of a pressure and air atomized nozzle for producing fine droplets of fluid. Through infrared thermography, we investigate temperature field distribution and heat flux evaluation on a heated SS-304 foil under various flow rates, heat fluxes, and fluid temperatures and nozzle to surface distance (N-SD). We are focusing mainly on the effect of different parameters in spray cooling at high heat flux such as nozzle to surface distance (N-SD), volumetric flow rate of fluid and fluid inlet temperature. Results show that AAN consistently achieves lower surface temperatures than PAN, demonstrating superior cooling efficacy. At 35°C and a flow rate of 0.1 L/min, AAN reduces average temperatures compared to PAN by 6.4°C, 7°C, and 6°C across heat fluxes ranging from 21.2 to 58.8 W/cm². The temperature decreases for each heat flux at a flow rate of 0.1 L/min and fluid inlet temperatures of 25°C and 35°C by 2.2°C to 11.2°C for the heat flux range of 21.2 to 58.8 W/cm² as the nozzle-to-surface distance increases from 20 mm to 30 mm. Infrared thermography offers localised insights of surface temperature distribution, which helps to evaluate accurate heat flux on substrate being heated.

Keywords: Spray cooling, Electronics cooling, Infrared thermography and Temperature field distribution, pressure atomized nozzles (PAN), air atomized nozzles (AAN)

1. Introduction

In today's modern environment, expecting electronic equipment to operate at high performance and speed requires a large amount of energy, which produces a large amount of heat. Device functionality depends on effective thermal management, yet conventional cooling techniques frequently cannot handle high heat fluxes.

To effectively dissipate high heat, direct liquid cooling such as spray cooling with water or dielectric liquids is used. When it comes to spray cooling, a number of factors are crucial in determining how well heat is removed from surfaces. First off, the cooling fluid's volumetric flow rate has a big impact on how quickly heat is transported. The distribution and coverage of the cooling spray are directly impacted by the nozzle's inclination angle and distance from the surface.

Additionally, the fluid's inlet temperature and thermo-physical properties, including its thermal conductivity, latent heat and specific heat capacity, affect its ability to absorb and dissipate heat effectively. The configuration of the spray nozzle, such as its shape and size of orifice, can also influence the spray pattern and coverage area. Furthermore, characteristics of the sprayed droplets, including their droplet size and velocity upon impact, play crucial roles in determining heat transfer efficiency. Environmental conditions, such as ambient pressure and temperature, further influence the cooling process. Moreover, surface temperature have significant effects on heat removal capacity. Understanding and optimizing these parameters are essential for maximizing the effectiveness of spray cooling systems in efficiently managing thermal loads in various applications. Thus this paper presents an initial investigation and is not intended as a comprehensive literature survey.

Spray cooling considered as one of the most efficient cooling methods in terms of heat removal and consumed power with same volumetric flow rate. Zhou et al.[1], and Gao and Li [2] studied the effects of parameters such as nozzle-to-surface distance and heat flux and pressure at inlet in spray cooling. Results showed that the primary factor influencing spray cooling performance was mass flow rate, with higher flow rates improving heat transfer. Additionally, it was discovered that 180° had the worst gravitational angle and that 30° to 120° had the best heat transfer.

The effectiveness of spray cooling using super-cooling water on a 10mm x 10mm square surface was experimentally investigated by Chen et al.[3]. The results showed that droplet velocity and mass flow rate, not sauter mean diameter (SMD), have a greater influence on the critical heat flux (CHF) and heat transfer coefficient in CHF.
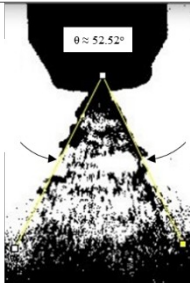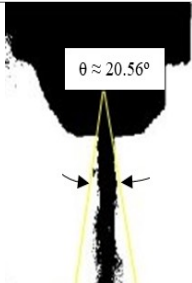
Salman and Khan [4] investigated the effects of surface temperature, nozzle-to-surface distance, and nozzle inlet pressure on a plain surface's thermal performance. The results of these investigations showed that the plain surface's spray cooling heat transfer performance improves significantly with increasing working fluid volumetric flow rate and decreasing nozzle-to-surface distance. Moreover, it was shown that droplet size and flow are mostly determined by the properties of the nozzle, meaning that temperature differences do not significantly affect droplet size. The forces acting on a droplet before to its contact on the heated surface alter, causing a modest increase in droplet velocity as the temperature difference grows. The way droplets interact with their surroundings in the spray chamber determines these forces.

Present study evaluates the performance of pressure atomized nozzles (PAN) and air atomized nozzles (AAN) in spray cooling for high heat flux applications. Experiments were conducted on a heated SS-304 foil using infrared thermography to measure temperature distribution at flow rates of 0.1 L/min and 0.2 L/min, fluid temperatures of 25°C and 35°C, and heat fluxes ranging from 21.2 to 58.8 W/cm². This study provides insights for optimizing spray cooling systems in thermal management applications.

2. Experimental Facility and Procedure

The experimental facility, which comprises a foil heater with DC power supply, spray nozzle, spray chamber, and data acquisition equipment, is depicted in the Fig.2 (a) both schematically and physically. A positive displacement gear pump (SHENCHEN, labGM) is used in the system to move water that is kept in a reservoir. A filter (Swagelok) is placed between the water reservoir and the pump to ensure no contaminants enter the flow loop, and a rotameter is used to measure the coolant's volumetric flow. A full cone nozzle (TG 0.3, Spraying Systems Co.) is utilised to generate the droplets. The nozzle configuration is detailed in the provided Table 1.

Table 1: Nozzle specifications

	Pressure atomized nozzle	Air atomized nozzle
Product code	TG-0.3	SU22B
Orifice diameter	0.51mm	-
Spray angle(degree)	50-61	18-21

For the heat transfer and PDPA experiments using a pressure atomized nozzle, we supplied fluid at rates of 0.1 and 0.2 L/min at room temperature, maintaining a nozzle-to-surface distance of 20 mm. The substrate is 40x80 mm² and is made of SS foil with a thickness of 100 microns. The SS foil used is SS-304, known for its high hardness, shine, wear resistance, and rustproof properties.

Joule heating is powered by an input power supply (TDK-Lambda) with a high current power source. Thermocouples and pressure transducers measure the temperature and pressure in the fluid flow loop through a data acquisition system (HIOKI LR8500). A high-speed infrared camera (FLIR X6900sc MWIR) along with a macroscopic lens is used to acquire

the temperature field of the heater foil's bottom surface. We are employing a macroscopic lens in a FLIR IR camera to analyse a 10x10 mm² area. With this specific lens, 1 pixel is equivalent to 0.0390625 mm for field measurement.

The experiments are repeated thrice for repeatability. The maximum uncertainty in the temperature field and heat flux field is ±1°C and ±7.05%, respectively.

The Fig.1 shows the heating setup, which includes a copper bus bar, Teflon plate, gaskets, DC power supply, and 100 µm thick SS foil. The electricity is passed through the foil by means of the high current DC power supply. There are two bus bar openings on the Teflon plate. A100 µm thick SS foil is sandwiched between the two silicon gaskets. The bus bars heat the foil as the DC power source sets the necessary current. A Hylam cover plate is placed above the gasket. A 10x10 mm portion of the foil is exposed at the top for spraying and the bottom surface of the heater foil is painted matte black using high-temperature-resistant black paint to increase the emissivity and minimize reflection and glare. The emissivity, thickness, and thermal conductivity of the black paint are 0.92, 10 µm, and 1.45 W/mK, respectively. The thermal images are captured at a frame rate of 1000 Hz.

1.Hylam plate(3 mm)
2.Gasket(2 mm)
3.SS foil(100 µm)
4.Gasket(2 mm)
5.Bus bars(20x40 mm²)
6.Teflon plate(214x122x10mm³)

Fig.1 Heater assembly

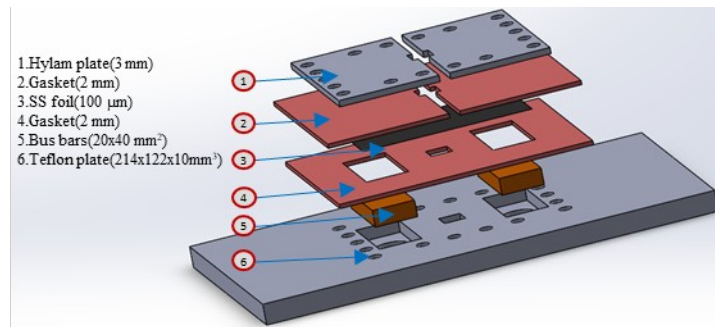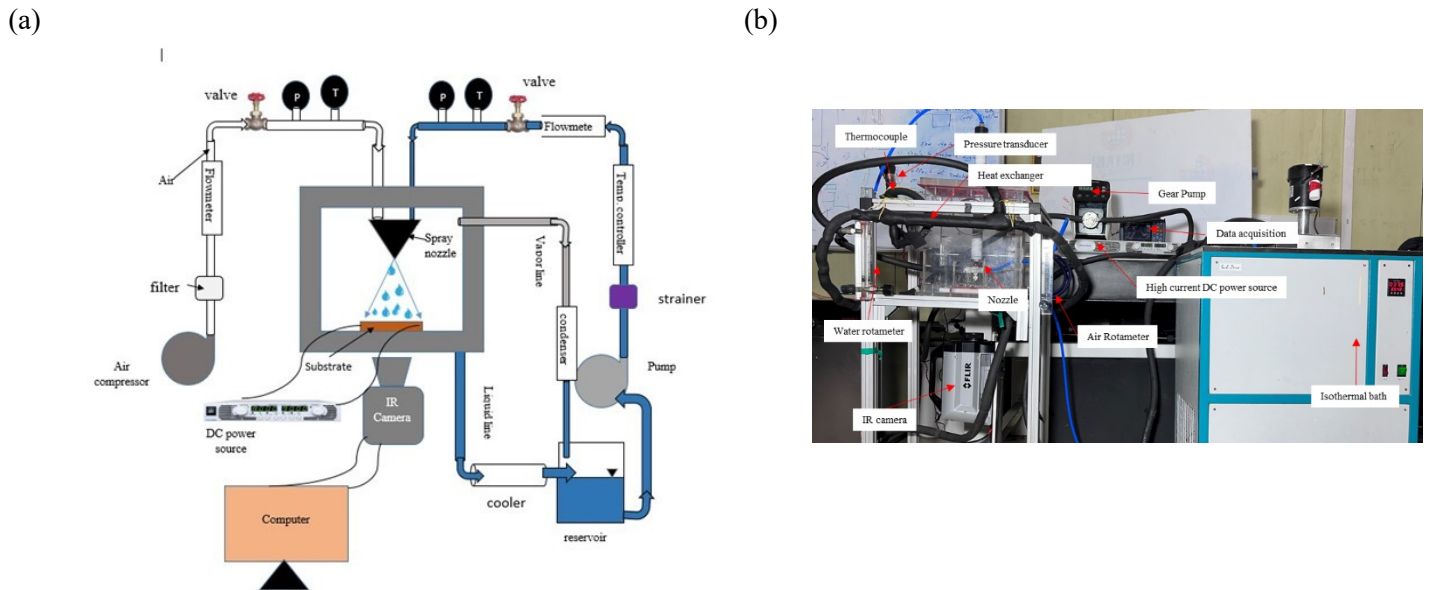(a)   (b)

Fig.2 (a) Schematic of Experimental setup (b) Actual Experimental setup

The first step is to calibrate the infrared camera at the required integration time (0.5 sec) and frame rate (1000 frames/s). The temperature data recorded from the infrared camera is smoothened to remove noise. The second step is to extract the heat flux field by performing pixel-wise energy balance on the heater foil temperature field. The illustration of energy balance at a pixel element for heat flux field is illustrated in Fig.3. The application of energy balance to the pixel element gives Equation (1).

$$Q_{stored} = Q_{gen} + Q_{cond} - Q_{rad} - Q_{conv} - Q_{fluid} \tag{1}$$
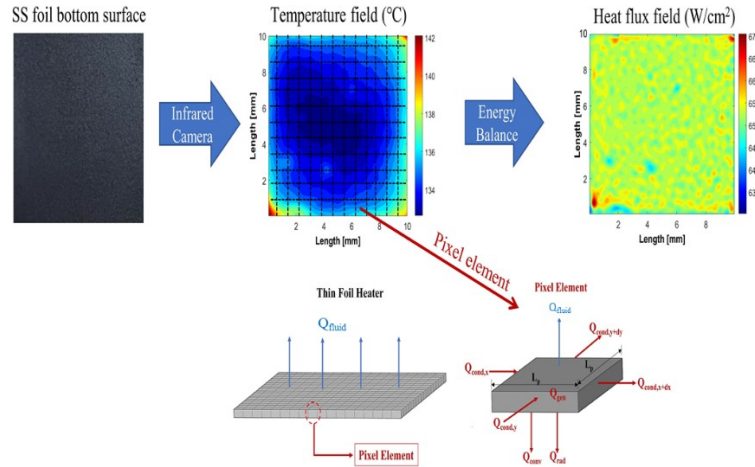
Fig.3. Illustration of energy balance at a pixel element for heat flux field

where fluid heat transfer is represented as Q_{fluid}[W]. Thus,

$$Q_{fluid} = Q_{gen} + Q_{cond} - Q_{rad} - Q_{conv} - Q_{stored} \tag{2}$$

The average fluid heat flux q_{fluid}, is calculated using the pixel element's length Lp as given in Equation (3)

$$q_{fluid} = \left(\frac{Q_{fluid}}{L_p^2} \right) \tag{3}$$

It is noted that Q_{stored} represents the change in energy of the surface due to cooling, and Q_{gen} being heat generated due to DC supply. While Q_{cond}, Q_{rad} and Q_{conv} are net conduction heat transfer along the surface, radiation and convection heat transfers underneath the surface respectively.

A MATLAB code is written to perform data processing and the energy balance on the temperature field of the heater foil surface that we get from the infrared camera.

3. Results and Discussion

3.1. Spray Characterisation:

This experiment uses a Phase Doppler Particle Analyser (PDPA) to characterise the spray. The probability of droplet dispersal as determined by PDPA is shown in the Fig.4. This non-invasive method allowed spray hydrodynamic characteristics, such as droplet diameter and velocity, to be determined without interfering with the spray process. The

Fig.4 presents the probability of droplet size distribution measured by PDPA at different flow rates and the probability of velocity distribution at different flow rates. PDPA measurements have been taken up to 21000 counts at room temperature (T_f = 26ºC) along the nozzle's axis and at the spray's two corner points.

From Fig.4 (a), most of the droplets fall within the range of 190 to 230 μm, with a SMD of 228.06 microns for a volumetric flow rate of 0.1 L/min at N-SD of 20mmfrom nozzle exit in PAN. From Fig.4 (b), On the other hand in AAN the SMD is 151.1 μm. From Fig.5 (a) for a volumetric flow rate of 0.2 L/min, the majority of droplet diameters range from 150 to 190 μm, with an SMD of 169.18 μm in PAN and From Fig.5 (b) AAN has the SMD of 116.6 μm. From Fig.4 (a) and Fig.5 (a), it is evident that increasing the volumetric flow rate from 0.1 L/min to 0.2 L/min results in a reduction in droplet diameter in PAN. Consequently, the SMD also decreases from 228.06 μm to 169.18 μm. Similarly, from Fig.4 (b) and Fig.5 (b), it is evident that increasing the volumetric flow rate from 0.1 L/min to 0.2 L/min results in a reduction in droplet diameter in AAN. Consequently, the SMD also decreases from 151.1 μm to 116.6μm.

As shown in Fig.4 (a), we can see the number of different droplet counts observed at different positions at certain N-SD and different flow rates for PAN. The measurements were done at one certain point, i.e., the nozzle centre, and different positions from the nozzle centre. It is observed that we get d_{32}=228.06 μm at V=0.1L/min, d_{32}=169.80 μm at V=0.2L/min. The total measured droplets at three different points at one particular N-SD, including the centre and two corner points, is included for PAN.

At a flow rate of 0.1 L/min, the droplet diameter distribution is wider and has a lower probability percentage compared to a higher flow rate for PAN. On the other hand, the droplet distribution is narrower and has a more probability percentage compared to the higher flow rate for AAN.

From Fig. 6(a), most of the droplet velocities fall within the range of 6.5 to 7.5 m/s, with an average velocity of 6.937 m/s for a volumetric flow rate of 0.1 L/min at a nozzle-to-surface distance (N-SD) of 20 mm for PAN from the nozzle exit.

From Fig. 6(b), average velocity is13.315 m/s at volumetric flow rate of 0.1 L/min and at a nozzle-to-surface distance (N-SD) of 20 mm for AAN from the nozzle exit, which is higher than average velocity of PAN.

Similarly, for a volumetric flow rate of 0.2 L/min, the majority of droplet velocities range from 12 to 16 m/s, with an average velocity of 12 m/s for PAN and average velocity of 18.969 m/s for AAN.

From Fig.6 (a) and Fig.7 (a), it is evident that increasing the volumetric flow rate from 0.1 L/min to 0.2 L/min results in an increase in droplet velocity for PAN. Consequently, the average velocity also rises from 6.937 m/s to 12 m/s. At a flow rate of 0.1 L/min, the droplet velocity distribution is narrower with a higher probability percentage compared to the distribution at a higher flow rate. At a flow rate of 0.2 L/min, the droplet velocity distribution is broader, with smaller droplets having a lower probability percentage.

In contrast to AAN, as shown in Fig. 6(b) and Fig. 7(b), increasing the volumetric flow rate from 0.1 L/min to 0.2 L/min results in a higher droplet velocity for AAN. Consequently, the average velocity increases from 13.315 m/s to 18.969 m/s. At a flow rate of 0.1 L/min, the droplet velocity distribution is wider with a lower probability percentage compared to the distribution at the higher flow rate.
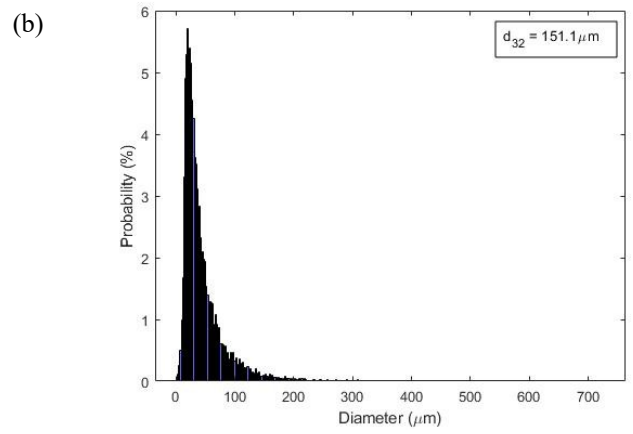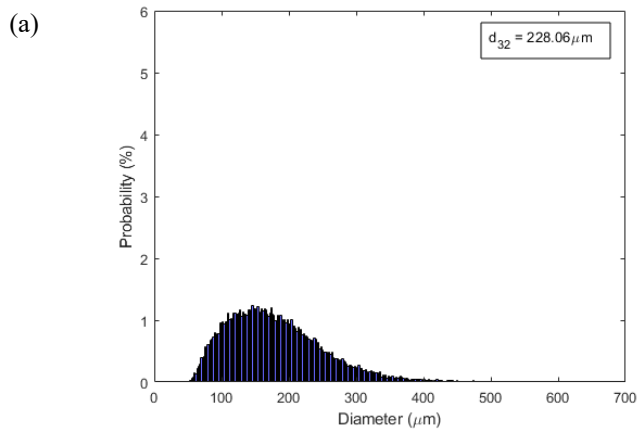
Fig.4. Probability of droplet diameter distribution at different flow rates at N-SD 20mm for $\dot{V}$=0.1 L/min (a) PAN (b) AAN
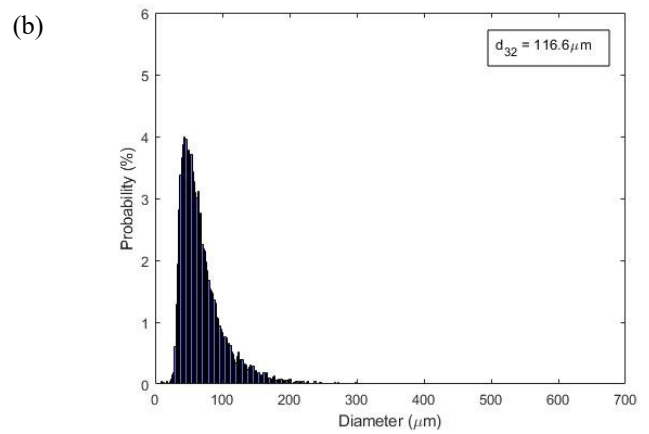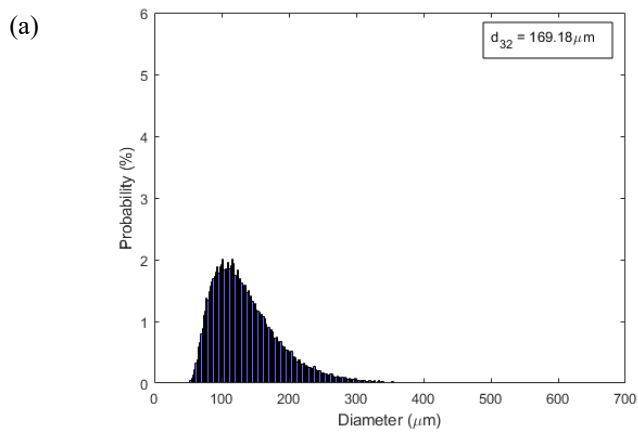

Fig.5. Probability of droplet diameter distribution at different flow rates at N-SD 20mm for $\dot{V}$=0.2 L/min (a) PAN (b) AAN
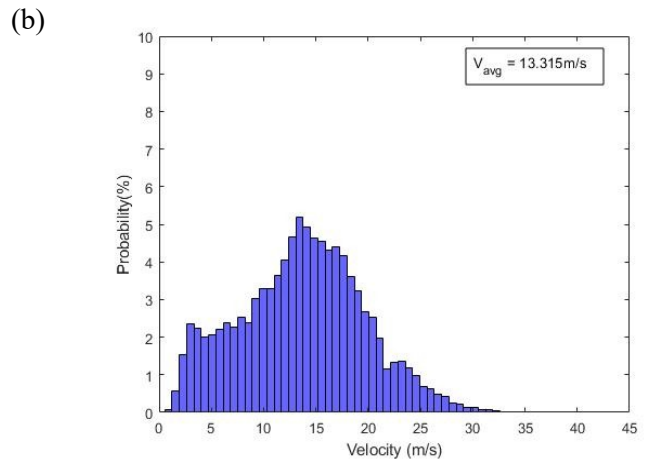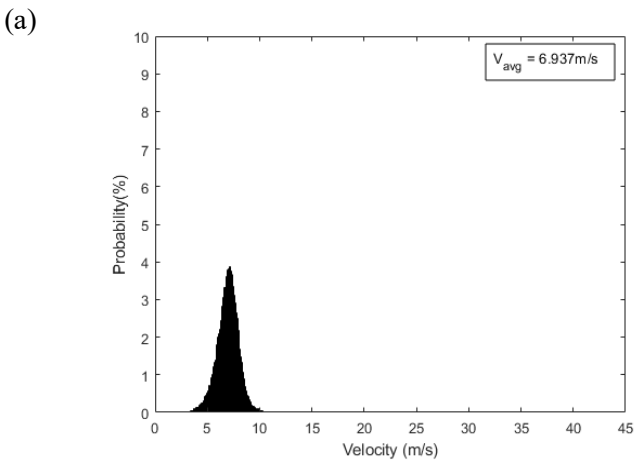
Fig.6 Probability of velocity distribution at different flow rates for at N-SD 20mm for $\dot{V}$=0.1L/min (a) PAN (b) AAN

(a)

(b)
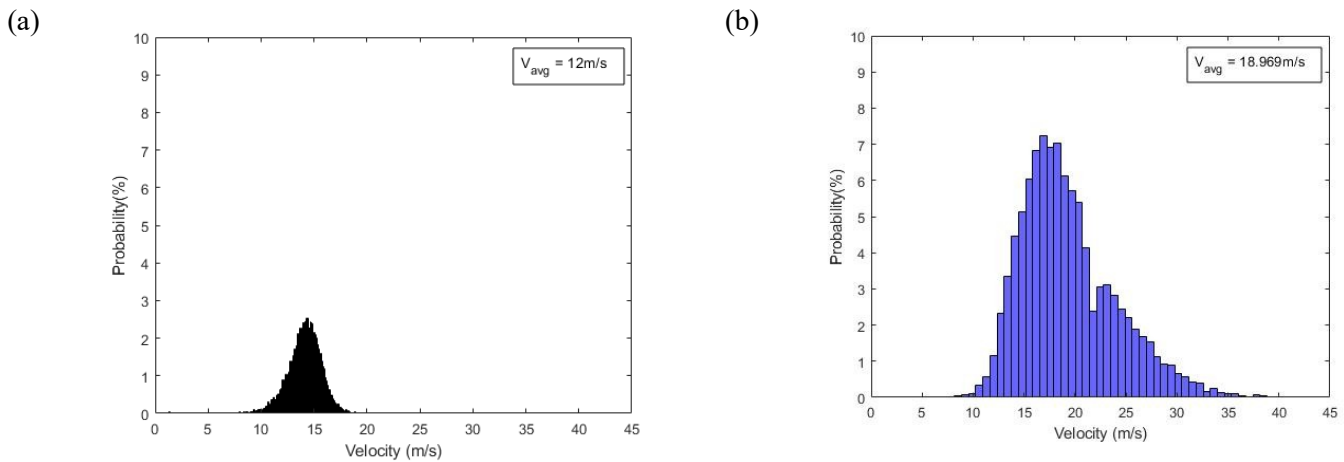

Fig.7 Probability of velocity distribution at different flow rates for at N-SD 20mm for $\dot{V}$=0.2L/min (a) PAN (b) AAN

The Fig.8 (a) illustrates the relationship between the SMD in (µm) and the flow rate in (L/min) at three different planes (5 mm, 10 mm, and 20 mm) from the nozzle in PAN. It is evident that the SMD decreases with an increase in flow rate for all measured planes. At the 5 mm plane, the SMD starts at 260 µm at a flow rate of 0.1 L/min and decreases to about 230 µm at 0.2 L/min. Similarly, the 10 mm plane exhibits a decrease in SMD from around 200 µm to 180 µm over the same range of flow rates, showing the smallest variation among the three planes. At the 20 mm plane, the SMD decreases from 240 µm to 200 µm as the flow rate increases. This trend indicates that higher flow rates promote better atomization, resulting in smaller droplet sizes. At the 5 mm plane, liquid near the nozzle exit interacts with the nozzle wall, resulting in thicker films and larger droplets. By the 20 mm plane, the spray becomes more developed, influencing breakup mechanisms. Secondary flows, such as swirling induced by nozzle geometry, create high shear regions around the 10 mm plane, leading to more aggressive droplet breakup and smaller SMD. Conversely, the 5 mm and 20 mm planes experience more droplet coalescence due to inter-droplet collisions, resulting in larger average droplet sizes and higher SMD.Conversely, Fig. 8(b) depicts the relationship between the SMD and the flow rate from the nozzle in AAN. It reveals that the SMD values are lower compared to those in PAN.

The Fig.9 (a) depicts the average velocity (in m/s) as a function of flow rate (in L/min) at three distinct planes: 5 mm, 10 mm, and 20 mm from the nozzle. As shown, the average velocity increases linearly with an increase in flow rate across all planes. At a flow rate of 0.1 L/min, the velocities are 6.8 m/s, 7.1 m/s, and 7.0 m/s for the 5 mm, 10 mm, and 20 mm planes, respectively. When the flow rate reaches 0.2 L/min, the velocities rise to around 10.5 m/s, 12.1 m/s, and 12.0 m/s for the 5 mm, 10 mm, and 20 mm planes, respectively. Notably, the velocity profile indicates that the velocity increases more steeply at the 10 mm and 20 mm planes compared to the 5 mm plane as the flow rate increases. This trend suggests that the atomization process enhances the spray dynamics further away from the nozzle, leading to higher velocities at greater distances for the same flow rates.

On the other hand, Fig.9 (b) shows the average velocity (in m/s) as a function of flow rate (in L/min) in AAN. The average velocities are higher compared to the PAN. At 10 mm, the spray may be in a transitional zone where the interaction between the droplets and the surrounding air, as well as turbulence, is more pronounced. This can lead to a redistribution of momentum among the droplets, causing a different velocity profile compared to the 5 mm and 20 mm planes.
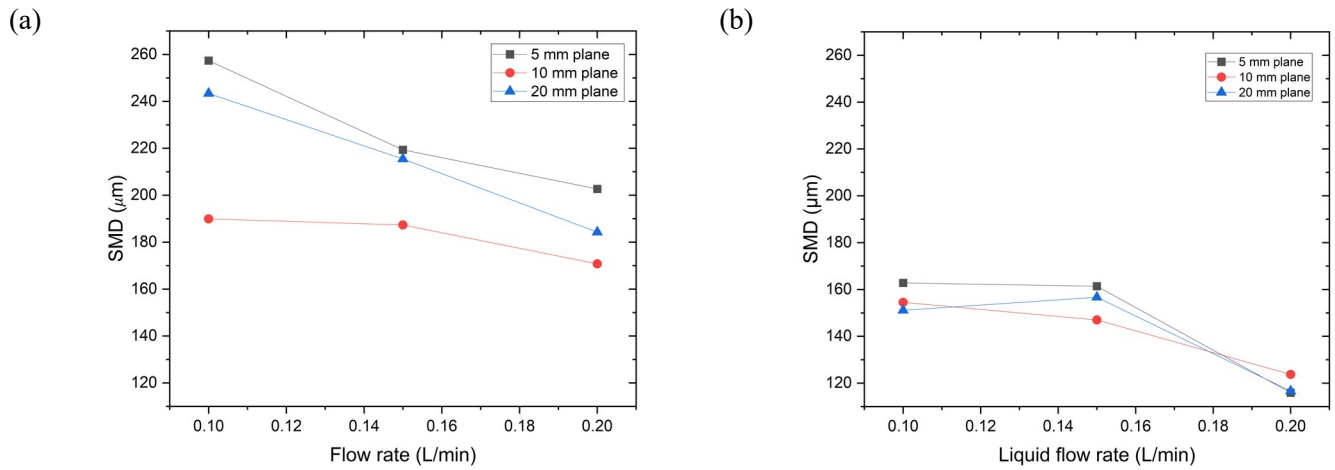
(a)

(b)

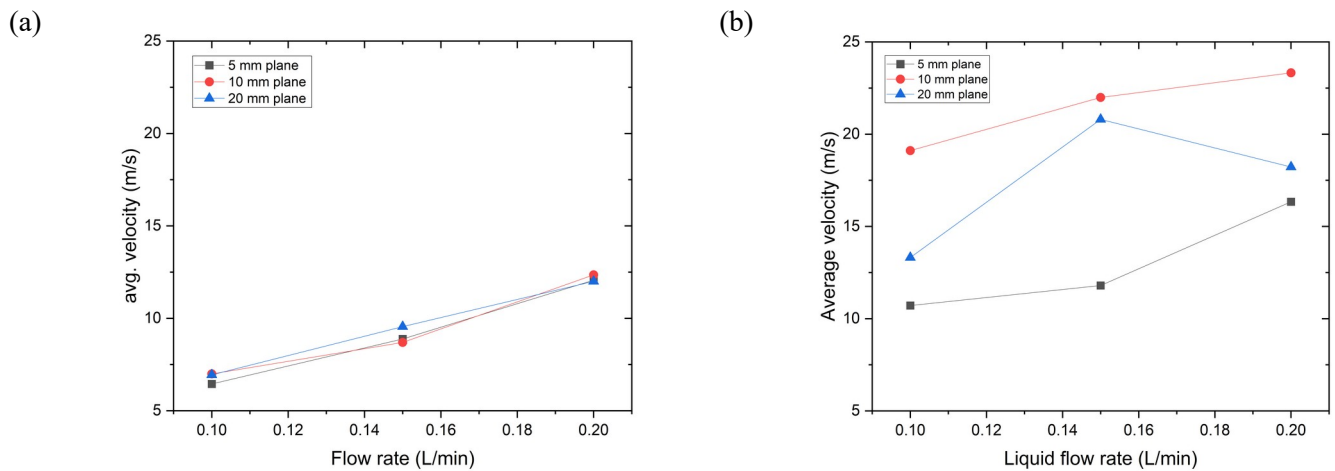Fig.8: Comparing flow rate at N-SD 5mm, 10mm and 20mm with SMD (a) PAN (b) AAN

(a)

(b)

Fig.9: Comparing flow rate at N-SD 5mm, 10mm and 20mm with average velocity (a) PAN (b) AAN

3.2 Field measurements of temperature and heat flux

The application of energy balance to the heater foil surface temperature determines the heat flux field. The field measurements for temperature and heat flux, corresponding to a heat flux of 58.78 W/cm² for a pressure atomized nozzle at a nozzle-surface distance (N-SD) of 20 mm and a flow rate of 0.1 L/min with an inlet fluid temperature of 25°C, are shown in the figure. These measurements are depicted in Fig.10 (a) and (b). The temperature and heat flux values obtained from the field measurements represent the spatial average of the temperature and heat flux fields.

Fig.11 shows field measurements of temperature for PAN and AAN at heat flux value of 58.78 W/cm². Fig.11 (a1), (a2) shows the comparison of PAN and AAN at $\dot{V}$=0.1 L/min, T_f =25°C. The temperature distribution as shown in Fig.11 (a1) shows a wider variation across the foil surface. This indicates that the heat is more unevenly distributed, with certain areas experiencing significantly higher temperatures.

Heater foil temperature (°C)   →   Heat flux(W/cm²)
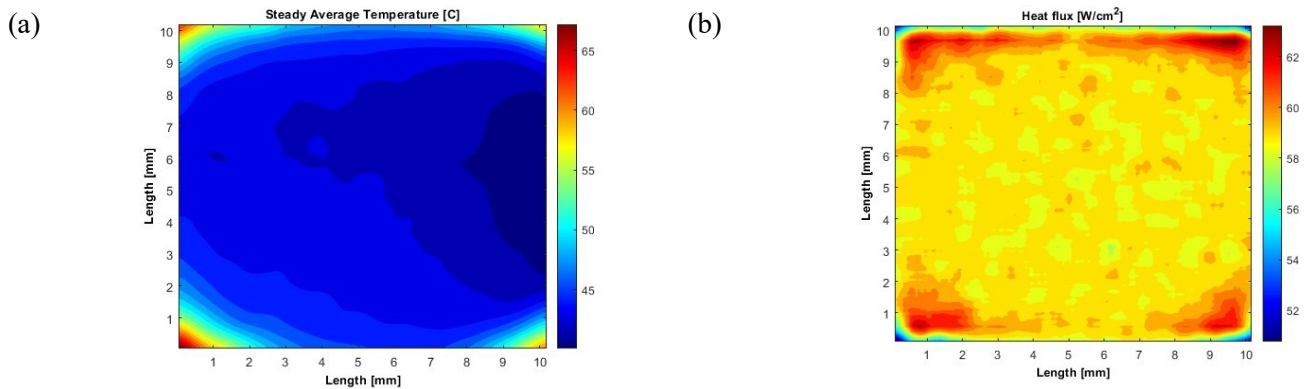
Fig.10 Field measurements for PAN $\dot{V}$=0.1L/min, 25°C of (a) Temperature (b) Heat flux

Fig.11 (a2) representing the AAN, exhibits a more uniform temperature distribution across the foil surface. The temperature range is narrower compared to the PAN, with most areas maintaining a steady temperature around 40°C to 45°C. This uniformity suggests that the AAN provides more efficient cooling, preventing localized overheating and promoting a more even thermal field.

In PAN, as shown in Fig.11 (b1), the temperature distribution ranges from approximately 40°C to over 65°C. The highest temperatures are concentrated near the central and upper regions of the plot, indicating less effective cooling in these areas. In contrast, the Fig.11 (b2) shows a temperature range that is generally lower, with a maximum temperature of about 50°C. The temperature distribution for the AAN is more uniform, suggesting a more effective and consistent cooling performance across the surface.

Fig.11 (c1) and (c2) shows the field measurement of temperature at $\dot{V}$=0.2 L/min and T_f=25°C for PAN and AAN. The central region maintains a consistent temperature range between 35°C and 45°C, with slight increases towards the edges. The AAN provides slightly better temperature uniformity and fewer hot spots, making it ideal for applications demanding highly consistent thermal management.

Fig.11 (d1) and (d2) compares PAN and AAN at inlet fluid temperature of 35°C and a flow rate of 0.2 L/min, the field measurements indicate that the temperature distribution is nearly identical for both the PAN and AAN configurations. This intriguing result suggests that under these specific conditions, the thermal behaviour of both systems is comparable. This observation warrants further investigation to understand the underlying mechanisms contributing to this similarity. Future studies will focus on exploring the factors influencing this temperature uniformity, such as the interaction between the spray characteristics and the surface properties, as well as any potential differences in the heat transfer dynamics.

3.3 Effect of inlet fluid temperature:

The Fig.12 (a) illustrates the relationship between foil surface temperature and heat flux for pressure atomized nozzles (PAN) and air atomized nozzles (AAN) at an inlet fluid temperature (T_f) of 25°C and 35°C with a flow rate $\dot{V}$=0.1 L/min and 35°C with a flow rate $\dot{V}$=0.1 L/min. At the T_f of 25°C, the foil surface temperature for the PAN is consistently higher than for the AAN at corresponding heat flux values. Specifically, at a heat flux of 21.18 W/cm², the surface temperatures are approximately 32°C for the AAN and 34.3°C for the PAN, showing a difference of 2.3°C. This trend continues for higher heat flux values, with the temperature difference increasing to 3.4°C at 37.64 W/cm² and 3°C at 58.78 W/cm². When the inlet fluid temperature is increased to 35°C, both nozzles exhibit higher surface temperatures compared to those at T_f of 25°C. The surface temperature difference between the PAN and AAN remains evident but varies with heat flux: 6.3°C at 21.18 W/cm², 7°C at 37.64 W/cm², and 6°C at 58.78 W/cm². These results indicate that the air atomized nozzle maintains a lower surface temperature compared to the pressure atomized nozzle, especially at lower heat flux values, highlighting the more effective cooling performance of the AAN under the tested conditions. These results indicate that the air atomized nozzle maintains a lower surface temperature compared to the pressure atomized nozzle, especially at lower heat flux values, highlighting the more effective cooling performance of the AAN under the tested conditions.
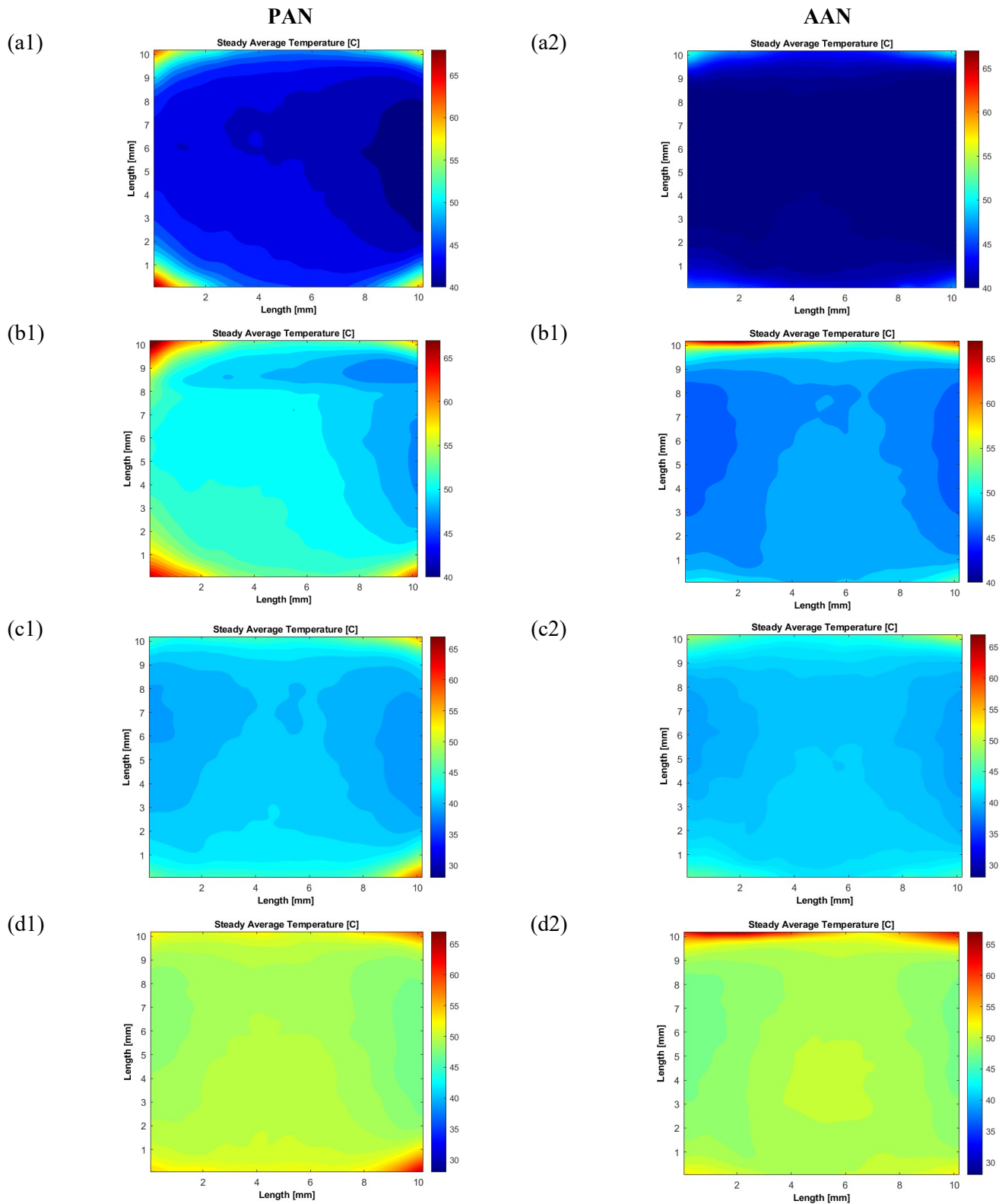
PAN

(a1)

AAN

(a2)

(b1)

(b1)

(c1)

(c2)

(d1)

(d2)

Fig.11 Field measurements of temperature for PAN and AAN (a1),(a2) at $\dot{V}$=0.1 L/min, T_f=25ºC (b1),(b2) at $\dot{V}$=0.1 L/min, T_f=35ºC (c1),(c2) at $\dot{V}$=0.2 L/min, T_f=25ºC (d1),(d2) at $\dot{V}$=0.1L/min,T_f=35ºC

For pressure atomized nozzles (PAN) and air atomized nozzles (AAN) at inlet fluid temperatures (T_f) of 25°C and 35°C with a flow rate $\dot{V}$=0.2 L/min and 35°C with a flow rate $\dot{V}$=0.2 L/min, the Fig.12 (b) shows the relationship between foil surface temperature and heat flux. The foil surface temperature of the PAN at similar heat flux values is consistently higher than that of the AAN at the T_f of 25°C. More specifically, the surface temperatures of the AAN and PAN are approximately 28°C and 29°C, respectively, at a heat flux of 21.18 W/cm², indicating a 1.5°C difference. At higher heat flux values, this tendency is maintained, and the temperature difference rises to 1.4°C at 58.78 W/cm² and 1.3°C at 37.64 W/cm².

When the inlet fluid temperature is increased to 35°C, both nozzles have greater surface temperatures than those at T_f of 25°C. The difference in surface temperature between PAN and AAN varies with heat flux: 1.4°C at 21.18 W/cm², 2.8°C at 37.64 W/cm², and 3.3°C at 58.78 W/cm². These results show that the air-atomized nozzle maintains a lower surface temperature than the pressure-atomized nozzle, particularly at lower heat flux values, showing the AAN's enhanced cooling capability under the studied conditions.
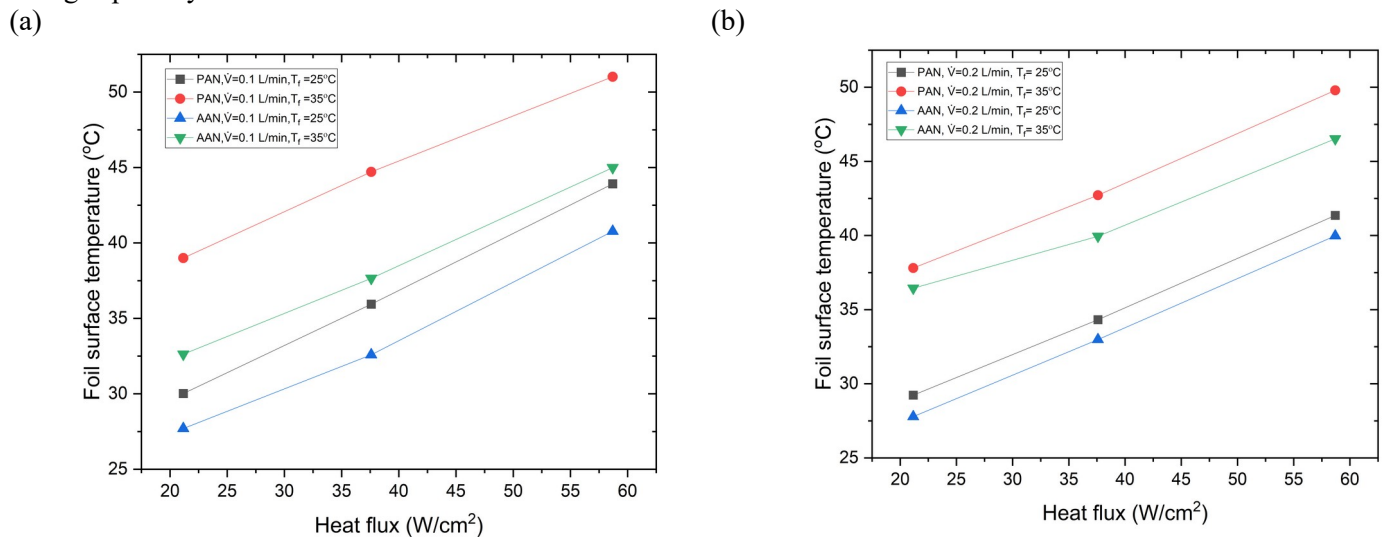
(a)   (b)

Fig.12 :Comparison of foil surface temperature for PAN and AAN at N-SD 20mm (a) $\dot{V}$= 0.1 L/min (b) $\dot{V}$= 0.2 L/min

3.4 Effect of nozzle to surface distances

The Fig.13 compares foil surface temperatures at N-SD =20mm and 30mm for a flow rate of 0.1 L/min of PAN at inlet fluid temperatures of 25°C and 35°C. When the inlet fluid temperature is 25°C, the temperature at N-SD 30 mm is consistently lower than N-SD 20 mm for the same heat flux values. At a heat flow of 21.18 W/cm², the surface temperatures of the N-SD 30mm and N-SD 20mm are about 28°C and 30°C, respectively, with a 2°C difference. The temperature difference increased to 5.9°C at 37.64 W/cm² and 11.1°C at 58.78 W/cm², indicating a continued trend towards higher heat flux values.

The Fig.13 (b) shows that for corresponding heat flux values, the temperature at a N-SD of 30 mm is consistently lower than at a N-SD of 20 mm at an inlet fluid temperature of 35°C. In particular, the surface temperatures for the N-SD 30 mm and N-SD 20 mm are about 35.8°C and 39°C, respectively, with a heat flux of 21.18 W/cm², suggesting a 3.2°C difference. With

the temperature difference rising to 6.6°C at 37.64 W/cm² and 10.2°C at 58.78 W/cm², this pattern continues at higher heat flux values. This is due to more uniform droplet dispersion, smaller droplet size, and reduced droplet velocity at the 30 mm distance. These factors contribute to better spreading, enhanced evaporation, and the formation of a more effective and stable thermal boundary layer, resulting in improved evaporative and convective heat transfer.

3.5 Effect of flow rate

Fig.14 (a) and (b) depicts the relationship between foil surface temperature and heat flux for PAN and AAN at T_f of 25°C and 35ºC with a flow rate $\dot{V}$=0.1 L/min and and $\dot{V}$=0.2 L/min. It can be clearly seen that in both the cases, the foil surface temperature for the PAN is higher than for the AAN at corresponding heat flux values. Fig.14 (a) depicts that if we increase flow rate from 0.1 L/min to 0.2 L/min at T_f =25ºC, PAN shows decrement of 1°C, 1.7 °C and 2.6 °C at respective heat flux of 21.18 W/cm², 37.64 W/cm² and 58.78 W/cm². Fig.11 (b) depicts that if we increase flow rate from 0.1 L/min to 0.2 L/min at T_f =35ºC, PAN shows decrement of 1.2ºC, 2 °C and 1.2 °C at respective heat flux of 21.18 W/cm², 37.64 W/cm² and 58.78 W/cm².
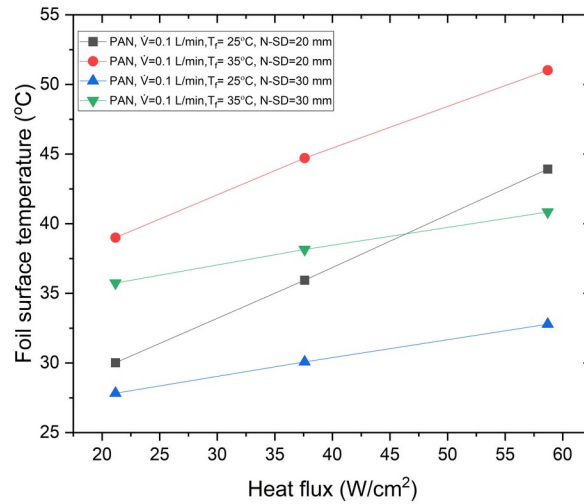

Fig.13: Comparison of foil surface temperature for PAN at N-SD = 20mm and 30 mm

Fig.14 (a) shows that when comparing the temperature change for AAN at flow rates of 0.1 L/min and 0.2 L/min, the temperatures approximately coincide at T_f = 25ºC and 35ºC for heat fluxes of 21.18 W/cm² and 37.64 W/cm², respectively. As the heat flux further increases to 58.78 W/cm², the temperature rises by 1°C at T_f = 25ºCand a flow rate of 0.2 L/min. Fig.14 (b) demonstrates that, at a flow rate of 0.2 L/min compared to 0.1 L/min, the temperature increases by 3.9°C, 2.3°C, and 1.5°C for heat fluxes of 21.18 W/cm², 37.64 W/cm², and 58.78 W/cm², respectively. These observations show contradictory results for the AAN case as we increase the flow rate. At low liquid flow rates, the air shearing the droplets is less effective, resulting in more air momentum directly striking the surface. This increased air momentum enhances the cooling effect on the surface.

The higher foil surface temperature with AAN at 35°C and 0.2 L/min is due to reduced droplet momentum (1.51×10^{-8} kg·m/s) despite increased velocity and smaller droplet size (D_{32} = 116.6 μm). This lower momentum diminishes the droplets' ability to penetrate the thermal boundary layer effectively. Additionally, the higher initial water temperature reduces the cooling gradient, while increased air entrainment and potential droplet coalescence further impede cooling efficiency, leading to higher surface temperatures.

Table 2: Momentum calculation for AAN

	0.1 L/min	0.2L/min
D_{32} (μm)	13.315	18.221
Velocity (m/s)	151.1	116.6
Mass (kg)	1.80×10^{-9}	8.30×10^{-10}
Momentum (kg.m/s)	2.40×10^{-8}	1.51×10^{-8}

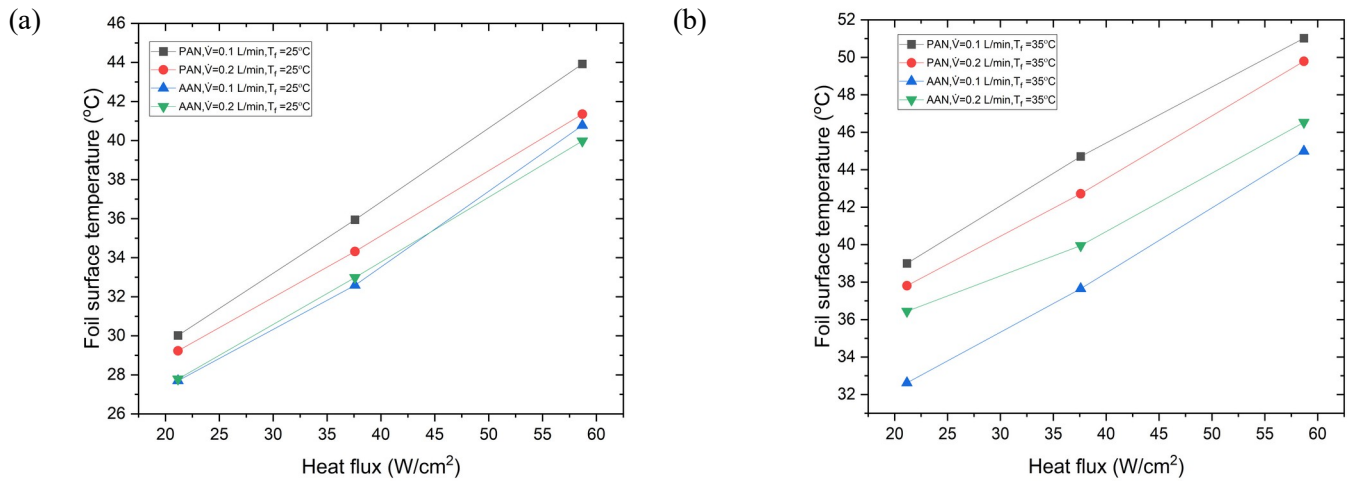(a)   (b)

Fig.14 Comparison of temperatures of PAN and AAN, at 0.1 L/min and 0.2 L/min for (a)T_f =25ºC (b) T_f =35ºC

4. Conclusion

1. Better cooling capabilities of AAN: Across all tested conditions, the aan consistently achieves lower average temperatures compared to the pan, indicating its superior performance in heat dissipation. This can be attributed to the finer droplet distribution and enhanced evaporation characteristics of the aan.
2. Impact of Fluid Inlet Temperature: Increasing the fluid temperature from 25°C to 35°C leads to a noticeable rise in average temperatures for both nozzle types. This suggests that higher fluid temperatures reduce the cooling efficiency, likely due to a diminished temperature gradient between the spray and the heated surface.
3. Flow Rate Efficacy: Interestingly, higher flow rates (0.2 L/min) result in higher average temperatures for AAN, contrary to what might be expected. Further investigation is required to study the underlying mechanism.
4. Heat Flux Dependence: As the heat flux increases from 21.2 W/cm² to 58.8 W/cm², average temperatures rise for both nozzles, which is expected due to the higher thermal load. However, the rate of temperature increase is less steep for the AAN, highlighting its better heat dissipation capability under higher thermal loads.
5. Research Implications: While AAN shows superior cooling performance under most conditions, the unexpected observation that higher flow rates lead to higher temperatures for AAN warrants further investigation. Factors such as droplet dynamics, air flow interaction, and thermal boundary layer stability should be explored to optimise the spray cooling system further.

REFERENCES

[1] N. Zhou, F. Chen, Y. Cao, M. Chen, and Y. Wang, "Experimental investigation on the performance of a water spray cooling system," *Appl. Therm. Eng.*, vol. 112, pp. 1117–1128, 2017.
[2] X. Gao and R. Li, "Effects of nozzle positioning on single-phase spray cooling," *Int. J. Heat Mass Transf.*, vol. 115, pp. 1247–1257, 2017.
[3] R. H. Chen, L. C. Chow, and J. E. Navedo, "Effects of spray characteristics on critical heat flux in subcooled water spray cooling," *Int. J. Heat Mass Transf.*, vol. 45, no. 19, pp. 4033–4043, 2002.
[4] A. S. Salman, N. M. Abdulrazzaq, A. Tikadar, S. K. Oudah, and J. A. Khan, "Parametric study of heat transfer characteristics of enhanced surfaces in a spray cooling system: An experimental investigation," *Appl. Therm. Eng.*, vol. 183, no. July 2020, p. 115824, 2021.
[5] N. Schweizer, "Multi-Scale Investigation of Nucleate Boiling Phenomena in Microgravity," 2010.
[6] G. Guggilla, R. Narayanaswamy, and A. Pattamatta, "An experimental investigation into the spread and heat transfer

dynamics of a train of two concentric impinging droplets over a heated surface," *Exp. Therm. Fluid Sci.*, vol. 110, no. September 2019, p. 109916, 2020.